SI Appendix:
Coordinated Beating of Algal Flagella is Mediated by Basal Coupling

Kirsty Y. Wan and Raymond E. Goldstein
Department of Applied Mathematics and Theoretical Physics,
University of Cambridge, Wilberforce Road, Cambridge CB3 0WA, UK

We discuss here in more detail aspects of flagellar synchronization and swimming gaits in the unicellular green algae described in the text and SI movies.

Pairwise synchrony: tri-flagellated CR mutant.

The *vfl3* mutant lacking or defective in distal striated fibers characteristically exhibits a variable number of flagella, each with apparently normal intrinsic motility but aberrant orientation. As a result, the flagella belonging to the same cell display greater frequency variance than the wildtype. When frequencies are sufficiently close, nearby configurations of flagella appear to be subject to significant hydrodynamic interactions. In the cell shown (Fig. S1) this leads to a competition between IP and AP components.

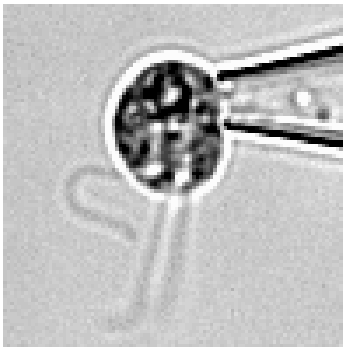

FIG. S1: Flagellar beating in the *vfl3* mutant. See also Movie S1 and Fig. 2D. A cell with three flagella: the inner pair is oriented with power strokes in the same direction and tends towards IP synchrony, while the "outer" flagellum (leftmost) attempts to synchronize in antiphase with respect to the first pair.

Pairwise synchrony: two VC somatic cells.

Here we elaborate on observed pairwise synchronization states between the flagella of two *V. carteri* somatic cells held in close proximity *and* with opposing power strokes, with particular emphasis on the consistency with theoretical predictions based on hydrodynamic interactions. As discussed in the main text, two states are observed (IP and AP), with the AP being preferred/more stable than the IP (Figs. 3 and S2). Transitions between IP and AP synchrony appear to be stochastic, stemming from inherent biochemical noise in the system. Within either state however, precise phase relationships are maintained. For interpolated flagellar phases $\phi_{1,2}$ ($\in [0,\ 2\pi]$) measured for each flagellum directly from the experimental data, we plot $\cos(\phi_{1,2})$ in Movies S2&3.

It is convenient and insightful to consider a dimension-reduced model in which each flagellum is modelled as a sphere of radius a constrained to oscillate along a near-circular trajectory of radius R [1]. Let $\hat{\mathbf{e}}_{\phi_i} = (-\sin(\phi_i), \cos(\phi_i))$ and $\hat{\mathbf{e}}_{r_i} = (\cos(\phi_i), \sin(\phi_i))$ denote unit vectors in the tangential and radial directions for each flagellum n, and measure phases $\phi_{1,2}$ CCW from the +ve x-axis. The two spheres are centered at $\mathbf{r_O}_{1,2}$, separated by $\ell = |\mathbf{r_O}_2 - \mathbf{r_O}_1|$ which is assumed large so that $a \ll \ell$ and $R \ll \ell$ (i.e. hydrodynamic far field), but simulations and experimental studies on colloidal systems have shown that qualitative predictions of the theory are still applicable even in situations where these values are not so small.

The velocities are given by $\mathbf{u}_i = \dot{R}_i\hat{\mathbf{e}}_{r_i} + R_i\dot{\phi}_i\hat{\mathbf{e}}_{\phi_i}$. The orbital radius is assumed to be flexible, characterized by a spring constant k and natural length R_0. Even for a simple driving force (assumed proportional to angular velocity), this flexibility allows each sphere to respond to hydrodynamic perturbations arising from the motion of its neighbor thereby leading to trajectory deformations of the correct sign to achieve synchronization. More generally, we can incorporate an additional variable driving force so that, for example,

$$\mathbf{F}_i = -k(R_i - R_0)\hat{\mathbf{e}}_{R_i} + F(\phi_i)\hat{\mathbf{e}}_{\phi_i}\ , \tag{1}$$

where

$$F(\phi_i) = F_0(1 - A\sin(2\phi_i)) \tag{2}$$

acting tangentially along the orbit [2]. The functional form of $F(\phi)$ has been chosen following Uchida & Golestanian [3] to provide the simplest modulated force for near-circular trajectories; terms of higher order become negligible. Depending on orbital rigidity one or the other of the two contributions will dominate [4]. For rapid synchronization of flagella, it has been shown that orbital compliance dominates over force modulation [5]. For counter-rotating spheres, if we take $F(\phi_1) = F_0(1 - A\sin(2\phi_1))$ then $F(\phi_2) = -F_0(1 + A\sin(2\phi_2)))$.

Motion is described [6] by the force balance $\mathbf{u}_i = \mathbf{O}_{ij}\mathbf{F}_j$, where

$$\mathbf{O}_{ij} = \zeta^{-1}\left(\delta_{ij} + (1-\delta_{ij})\frac{3a}{4r_{ij}}\left(1 + \frac{\hat{\mathbf{r}}_{ij}\hat{\mathbf{r}}_{ij}}{r_{ij}^2}\right)\right), \quad (i,j = 1,2) \tag{3}$$

where $\zeta = 6\pi\eta a$ is the drag coefficient of a sphere and $\hat{\mathbf{r}}_{ij} = (\mathbf{r}_j - \mathbf{r}_i)/r_{ij} \simeq \hat{\mathbf{x}} + \mathcal{O}(R/\ell)$. Force balance in the tangential

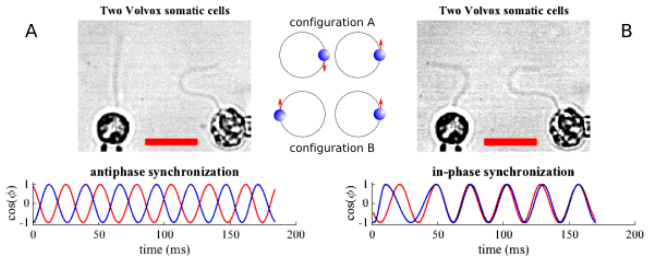

FIG. S2: Synchronization of flagella on *Volvox* somatic cells. As each flagellum is on a separate pipette-held cell, coupling is solely through the intervening fluid. The beating patterns correspond to configurations of counter-rotating spheres which tend to (A) AP or (B) IP states; state A is more stable and has a higher frequency than B, as predicted. See Movies S2&3. Scale bars are 10 μm.

and radial directions gives:

$$\zeta \dot{R}_i = \epsilon\left(1 + \hat{\mathbf{x}}\hat{\mathbf{x}}\right)\mathbf{F}_i \cdot \hat{\mathbf{e}}_{R_i} - k(R_i - R_0) \tag{4}$$
$$\zeta R_i \dot{\phi}_i = F(\phi_i) + \epsilon\left(1 + \hat{\mathbf{x}}\hat{\mathbf{x}}\right)\mathbf{F}_i \cdot \hat{\mathbf{e}}_{\phi_i} \ ,$$

where $\epsilon = 3a/4\ell$. If radial variations decay much faster than tangential ones, so $\dot{R} \simeq 0$, then $k(R_i - R_0) \sim \mathcal{O}(\epsilon)$, and we can further expand $\mathbf{F}_i/\zeta \approx R_i\dot{\phi}_i\hat{\mathbf{e}}_{\phi_i} + \mathcal{O}(\epsilon)$. The dynamics of oscillator 1 is then given by

$$\begin{aligned}\zeta\dot{\phi}_1 =& F_1(\phi_1) + \frac{\epsilon F_i(\phi_i)}{2R_0}[3\cos(\phi_1 - \phi_2) - \cos(\phi_1 + \phi_2)] \\ &- \frac{\epsilon F_i(\phi_i)F_j(\phi_j)}{2kR_0^2}[3\sin(\phi_1 - \phi_2) - \sin(\phi_1 + \phi_2)] \ ,\end{aligned} \tag{5}$$

and similarly for oscillator 2 under interchange of $1 \leftrightarrow 2$.

For counter-rotating spheres the phase sum $\Xi = \phi_1 + \phi_2$ fluctuates about $\Xi_0 = 0$ or $\Xi_0 = \pi$ in either AP or IP states. In the case of AP synchrony, let $\Xi = \Xi_0 + \delta$, then $\phi_2 = \phi$, and $\phi_1 = \delta - \phi$, and we have

$$\begin{aligned}\zeta\frac{\dot{\delta}}{\delta} \simeq& -2\frac{F_0 A}{R_0}\cos(\phi) - \frac{\epsilon F_0 A}{R_0}\cos(2\phi)(3\cos(2\phi) - 1) \\ &- \frac{\epsilon F_0^2}{kR_0^2}(1 + A\sin(2\phi))^2 \ ,\end{aligned}$$

and similarly for the IP state - for a change of sign to the last term in the above. This last term corresponds to elastic deformation of orbits, and is < 0 (leading to stability) for all phases ϕ in the case of AP synchronization but > 0 (leading to instability) in the case of IP synchronization, consistent with our experimental observations. Furthermore the average period $T_{\text{AP, IP}}$ of these metastable states is then given by $\int_0^{2\pi} \dot{\phi}^{-1}\, d\phi$ [7, 8]:

$$T_{\text{AP, IP}} = \frac{2\pi\zeta R_0}{F_0\sqrt{1 - A^2}}\left(1 \mp \frac{1}{2}\epsilon\right) \ . \tag{6}$$

From the data, we find the experimental configuration to be consistent with $a \simeq 3$ μm for a separation of $\ell \simeq 15$ μm; in particular, the AP state is indeed faster than the IP.

Mechanical perturbation of flagellar beating

The marine quadriflagellate *T. suecica* swims with a characteristic transverse gallop (Fig. 4) when free or pipette-held. The presence of theca renders them amenable to micromanipulation. Movie S4 compares a pipette-held cell with flagella that are free to beat, with the same cell some time later after beating is stalled in one of its four flagella by careful application of suction (which traps the flagellum inside the pipette). The prior coordination in the remaining flagella is retained despite the significant change in hydrodynamic loading.

Systematics and ultrastructure of the green algae.

The species of green algae referenced in this study are presented in full in Fig. 5. Here, we provide some additional details and references for the interested reader.

According to the most current classification, the Viridiplantae comprises two phyla: the Streptophyta – which contains many freshwater Charophyta algae and most land plants, and the Chlorophyta – which is the relevant category for most green algae. The precise evolutionary history of the Chlorophyta has proved rather difficult to elucidate, in the current consensus there are three core classes (Chlorophyceae: C, Trebouxiophyceae: T, and the Ulvophyceae: U), and a fourth non-monophyletic class of more primitive algae known collectively as the "Prasinophyceae".

Earlly attempts to classify the green algae by morphological form (unicellular, colonial, filamentous) [9] were superseded by schemes based on comparisons of basal body (BB) ultrastructure (microtubular roots, orientation of basal bodies etc) [10–12]. The Prasinophyte algae have counter-clockwise offset of basal bodies (now considered a primative trait), while in contrast the Chlorophyte algae are characterized by a clockwise offset (see for instance *Chlamydomonas*, Fig. 1D). Later molecular approaches soon became available. Genetic markers based on ribosomal (SSU rDNA) or chloroplast genes such as *rbc*L were used to verify and refine existing classifications. These were particularly important for distinguishing between species that were otherwise morphologically identical [13]. Phylogenetic trees are then constructed based on these results via statistical methods such as maximum likelihood or maximum parsimony. The branching order and relative edge lengths shown on Fig. 5 were estimated from a composite of available maximum likelihood trees [13–20].

Most of the Prasinophyte algae considered in this study belong to the order Pyrmimonadales which reside at the base of the Chlorophyta and are considered to be the earliest green algae [11]. These phytoflagellates have 4 to 16 flagella and are united by their lack of advanced Chlorophycean characters as well as by the presence of primitive scaly body coverings. The *Pyramimonas* genus, first described from a freshwater locality

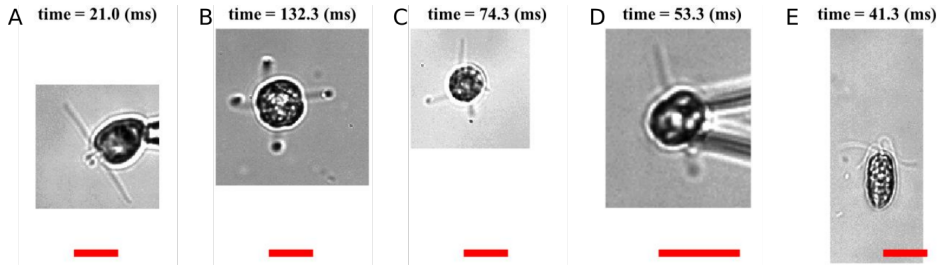

FIG. S3: Distinct quadriflagellate gaits. See Fig. 6 of text and Movie S6. (A) trot (*Pyramimonas parkeae*) held stationary by a micropipette, (B) pronk (*Pyramimonas tetrarhynchus*), (C) rotary gallop of *Carteria cruicifera* and of *Tetraselmis suecica* viewed apically when (D) held by micropipette or (E) freely-swimming. Scale bars are 10 μm.

in Cambridge, England, has been shown to exhibit great morphological variability not just in the numbers of flagella but also the composition of types of organic scales (crown, square, box etc). According to *rbcL* sequencing, *Pyramimonas* does not constitute a monophyletic clade. At least four subgenera exists, namely *Pyramimonas*, *Vestigifera*, *Punctuate*, and *Trichocystis*, of these all four Pyramimonas species studied here (*P. parkeae*, *P. tetrarhynchus*, *P. octopus*, and *P. cyrtoptera*) belong to the same subgenus *Pyramimonas* [21]. Chloroplast sequencing has also revealed accelerated rates of evolution in this monophyletic subgenus. The branching order among these four species is presented in Fig. 5, following Daugbjerg *et al* [16], and Harðardéttir *et al* [22]. Only *P. tetrarhynchus* (the type species) is a freshwater species, the other three being marine. The prototypical *Pyramimonas* has four homodynamic and isokont flagella which emerge from an anterior pit, where the two oldest BBs are connected by a large synistosome which is striated in cross-section and thought to be contractile. Flagella beat away from each other in a roughly cruciate pattern, with some differences across species in the precise geometry of the four BBs, which form a diamond shape in most cases.

The final Prasinophycean alga in our list is *Tetraselmis* [12] (synonymous with *Platymonas*). It is considered very basal to the UTC clade, has a counterclockwise orientation of BBs, and is associated with early evolution of the plant phycoplast which is essential for the later emergence of multicellularity within the Chlorophyta. Along with *Scherffelia*, *Tetraselmis* is classified under the order Chlorodendrales [23, 24], which comprises thecate scaly flagellates, and were among the first green flagellates to evolve a rigid wall (theca). The presence of this bounding wall is thought to have prevented cell division in the flagellate state, and distinguishes *Tetraselmis* from most other Prasinophytes, which divide while remaining fully motile. In electron micrographs, the nucleus appears to be positioned centrally between the flagellar apparatus and pyrenoid.

The Chlamydomonadalean algae form the largest Chlorophyceae group and is taxonomically complex and diverse [14, 15]; of the species studied here the genus *Carteria* is the most basal according to molecular phylogenetics, supporting the notion that the common ancestor of the core Chlorophyte algae may have been a Carteria-like quadriflagellate [20, 25]. The biflagellate condition of *Chlamydomonas* may have resulted from a subsequent reduction from four flagella to two. Biflagellate Chlamydomonadales possess a CW rotation of the flagellar apparatus, and comprises mainly freshwater and terrestrial species. The favored species *Chlamydomonas reinhardtii* and its multicellular relative *Volvox carteri* have been extensively studied as model organisms exemplifying the evolution to multcellularity (see also [25] and the many references therein). While many of these species are photoautotrophic, harnessing sunlight for energy through photosynthesis, a number have evolved into obligate heterotrophs which make use of various carbon sources. These include the colourless and wall-less algae *Polytoma* and *Polytomella* [26, 27], which through the loss of chloroplasts have rather unusual mitochondrial or plastid genomes [28]. In particular *Polytomella* has lost their plastid genomes entirely [29], but is thought to be closely related to the photosynthetic species *V. carteri* and *C. reinhardtii*.

In Fig. 5, the illustrations of the basal apparatus represent simplified planar views only, please refer to the following external references for the detailed ultrastructure of each species featured in this work. i) *Pyramimonas parkeae* [30, 31], ii) *Pyramimonas tetrarhynchus* [32, 33], iii) *Pyramimonas octopus* [34–36], iv) *Pyramimonas cyrtoptera* [37], v) *Tetraselmis suecica* and *T. subcordiformis* [38, 39] vi) *Carteria crucifera* [40] (the basal apparatus of *Carteria* Group 2 is most peculiar, in which sigmoid shaped electron dense rods extend between opposite BB pairs) vii) *Chlamydomonas reinhardtii* [41], dikaryon [42] viii) *Volvox carteri* [43, 44] ix) *Polytoma uvella* [45] (and for *Polytoma papillatum* [46]) x) *Polytomella parva* (synonymous with *P. agilis*) [47] . In particular unlike the BBs of *Pyramimonas* which emerge almost parallel from a grove inside the cell, the BBs of Chlorophycean algae are often tilted with respect to each other, for instance the two BBs of *C. reinhardtii* are oriented at $70-100^\circ$ [41] and those of *P. uvella* at 140° [46]. BBs have also been numbered throughout according to the convention of Moestrup [36] by order of ontogenetic age wherever such information was available.

Swimming with four flagella.

Select species of quadriflagellates exemplify the possible gait symmetries. The motion is highly species-specific, where the patterns or sequence of actuation of the flagella appear to

be independent of whether or not the cell body has been fixed in place.

Flagellar synchronization in a dikaryon of *Chlamydomonas*.

Although CR is most likely to occur in its vegetative state, gametic cells capable of sexual reproduction can form under nitrogen deprivation in the presence of light. When two biflagellate CR gametes of opposite mating types (+ and −) come together, flagellar agglutination [48] occurs whereby the flagella of opposite mating types adhere strongly to each other (Figure. S4A1). This is followed by autolysin secretion which digests away the cell walls, after which a fertilization tubule extends from the + gamete to its partner (Figure. S4A2). If fusion is successful, a single temporary dikaryon is formed, which is quadriflagellate (Figure. S4A3).

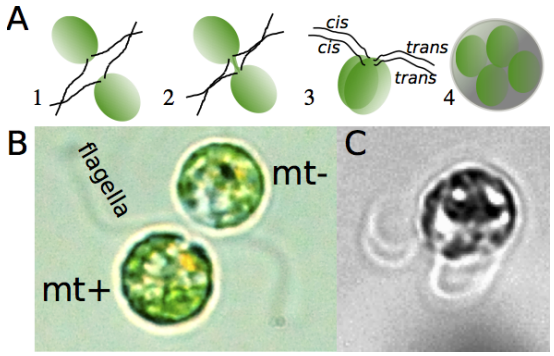

FIG. S4: Generation of a dikaryon of *Chlamydomonas*. For brevity, eyespot locations are not shown. (A) 1-4: Life cycle of sexual reproduction in CR. (B) A pair mating (stage 1). (C) A quadriflagellate dikaryon is formed. See Movie S5.

These dikaryons exhibit a striking double bilateral breaststroke (in contrast to the double cruciate breaststroke observed in *P. parkeae*), in which pairs of flagella on the same side become strongly phase-synchronized. It is known that the flagella separate distally into *cis-cis* and *trans-trans* pairs, allowing cells to remain strongly phototactic during this period, which is another indication of good flagellar coordination. No new synthesis of basal body fibers occur, and indeed all traces of basal bodies and associated rootlets and fibers dissolve within 6 hours after mating [49]. Therefore there is a strong asymmetry in internal connectivity immediately upon formation of the quadriflagellate zygote, prior to the dissolution of the distal fibers between the original BBs (of like mating type), but lack of physical connections between pairs of BBs of unlike mating type (recall Fig. 5). Eventually, maturation of the zygotes leads to resorption of all flagella, and formation of a CR spore. These diploid zygotes await favorable conditions before release of 4 new haploid progeny, whereupon BBs are reassembled *de novo*.

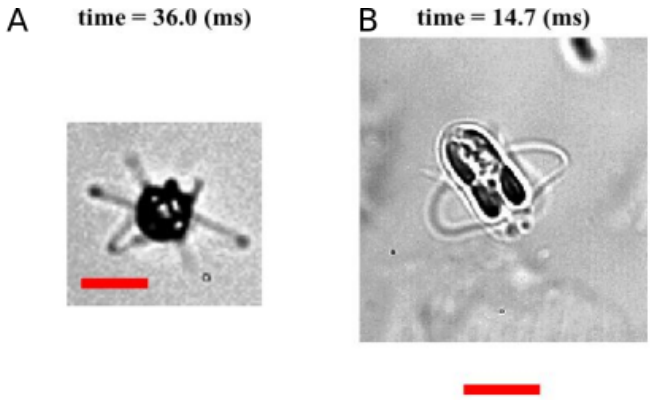

FIG. S5: Swimming dynamics of the octoflagellate *P. octopus*. (A) Top view: cell is observed to rotate CCW about its long axis over time, and side view (B), where several pairs of in-phase breaststrokes are observed, principally between diametrically opposed flagella. See Movie S7. Scale bars are 10 μm.

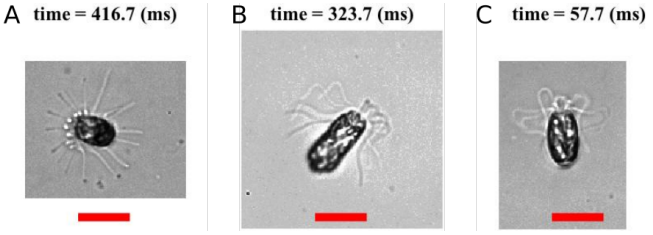

FIG. S6: Distinct hexadecaflagellate gaits. (A) Pronk: all flagella synchronized (a hydrodynamic mode). (B) bilateral: one group comprising half of the flagella are synchronized, but are in anti-phase relative to the complementary group. (C) mixed mode: resembles a *P. octopus*. See Movie S8. Scale bars are 20 μm.

Swimming with eight flagella.

The octoflagellate *P. octopus* displays stochastic switching between a number of different gaits (Fig. S5 and Movie S7). Primary among these is a complex breaststroke which appears to involve a number of phase-shifted pairwise IP breaststrokes. The IP synchrony within certain of the pairs are more robust than in others (the basal architecture is far from radially symmetric, with the large synistosome connecting BB1 and 2 (see Fig. 5).

Swimming with sixteen flagella.

Flagellar coordination in the hexadecaflagelalte *P. cyrtoptera* leads to a number of distinctive gaits which may be dependent on the current state of contractile of the fiber network: three of which are shown here (Fig. S6 and SI Video 7. (A) Significant nearest-neighbour hydrodynamic effects can synchronize all sixteen flagella, which pronks with a well defined periodicity coinciding with the beat frequency of an individual flagellum. (B) The underlying basal-body network exhibits significant bilateral symmetry (Fig. 5), which could

explain the frequent appearance of a bilateral gait in which flagella are divisible into two groups, which beat alternately. Flagella within each group appear to be strongly coupled in IP by hydrodynamic interactions. As a result the cell body sways periodically from side to side. C) In certain individuals, basal coupling appears strong enough to permit several phase-shifted breaststroke pairs and swimming is reminiscent of an octoflagellate with flagella doubled up in pairs - with the flagella in each pair undulating in perfect unison.

Emergence of metachronism in a hexadecaflagellate

In *P. cyrtoptera*, neighboring flagella experience strong hydrodynamic interactions due to their close spatial proximity, giving rise to the striking pronking gait (Movie S8) in which all sixteen flagella beat with zero relative phase difference. In this organism yet another phenomenon can be attributed to hydrodynamic synchronization: occasionally, we observe metachronal waves propagating circumferentially around the crown of flagella which become especially notable in cells swimming close to surfaces. We discuss below how this is consistent with theory concerning fluid-structure interactions near no-slip surfaces, and where dynamics are dominated by orbital compliance (Fig. S7).

Firstly, steric interactions near the wall forces the flagella to 'flatten' or reorient more laterally, contrary to the normal state in which they are recurved longitudinally along the cell body from the anterior to the posterior. This new orientation becomes more conducive to hydrodynamic coupling (see reference Brumley *et al* [14] of main text) between the flagella (Fig. S7A). Interactions are maximised when flagella are placed side-by-side and minimized when placed in the up/downstream directions. Secondly, proximity near the no-slip boundary itself means that the nearest-neighbor contribution to the coupling is increased, again encouraging the emergence of metachronal waves.

For the cell shown, a symplectic metachronal wave propagates CCW among its flagella, which causes the cell to rotate very slowly in a CW sense. We take the optical flow field $\mathbf{U}(\mathbf{r};t)$ as proxy for the real flow field in the vicinity of the organism (there is good agreement in direction even if flow magnitudes are less reliable). The time averaged flow field (Fig. S7) is clearly rotary

$$\langle \mathbf{U}(\mathbf{r};t) \rangle = \frac{1}{t}\int_0^t \mathbf{U}(\mathbf{r};t)\,dt$$

We decompose the flow into its radial and tangential components

$$\mathbf{U}(\mathbf{r};t) = U_r(\mathbf{r};t)\mathbf{e}_r + U_\theta(\mathbf{r};t)\mathbf{e}_\theta \tag{7}$$

and concentrate on the radial component which corresponds the direction perpendicular to the wall, since forces perpendicular to a wall decay much faster than the tangential contribution. The plots reproduce features distinctive of a metachronal wave.

[1] Niedermayer T, Eckhardt B, Lenz P (2008) Synchronization, phase locking and metachronal wave formation in ciliary chains. *Chaos* 18 (037128)

[2] Uchida G, Golestanian (2012) Hydrodynamic synchronization between objects with cyclic rigid trajectories. *The European Physical Journal E* 35: 1-14

[3] Uchida N, Golestanian R (2011) Generic Conditions for Hydrodynamic Synchronization. *Phys. Rev. Lett* 106 (058104)

[4] Kotar J, Debono L, Bruot N, Box S, Philips DB, Simpson SH, Hanna S, Cicuta P (2013) Optimal hydrodynamic synchronization of colloidal oscillators.*Phys. Rev. Lett* 111 (228103)

[5] Brumley DR, Polin M, Pedley TJ, Goldstein RE (2012) Hydrodynamic synchronization and metachronal waves on the surface of the colonial alga *Volvox carteri*. *Phys. Rev. Lett* 109 (268102)

[6] Happel J, Brenner H (1983) Low Reynolds number hydrodynamics: with special applications to particulate media. *Kluwer, New York*

[7] Box S, Debono L, Philips DB, Simpson SH (2015) Transitional behavior in hydrodynamically coupled oscillators. *Phys. Rev. E* 91 (022916)

[8] Bruot N, Kotar J, de Lillo F, Cosentino Lagomarsino M, Cicuta P (2012) Driving potential and noise level determine the synchronization state of hydrodynamically coupled oscillators *Phys. Rev. Lett* 109 (164103)

[9] Blackman F (1900) The primitive algae and the Flagellata. *Annals of Botany* 14: p647-688.

[10] Irvine D, John D (1984) Systematics of the green algae *Academic Press, Oxford, England*

[11] O'Kelly CJ, Floyd GL (1984) Flagellar apparatus absolute orientations and the phylogeny of the green algae. *Biosystems*16: p227-251

[12] Mattox K, Stewart K (1984) Classification of the green algae: a concept based on comparative cytology. *Systematics of the green algae. The Systematics Association Special Volume 27, Academic Press, London and Orlando* p29-72

[13] Pröschold T, Leliaert F (2007) Unravelling the algae: the past, present, and future of algal systematics (Chapter 7, Systematics of the green algae: conflict of classic and modern approaches) *CRC Press*

[14] Nakada T, Misawa K, Nozaki H (2008) Molecular systematics of the Volvocales (Chlorophyceae, Chlorophyta) based on exhaustive 18S rRNA phylogenetic analyses *Mol. Phylogenet. Evol* 48: 281-291

[15] Nozaki H, Misumi O, Kuroiwa T (2003) Phylogeny of the quadriflagellate Volvocales (Chlorophyceae) based on chloroplast multigene sequences *Mol. Phylogenet. Evol* 29: 58-66

[16] Daugbjerg N, Moestrup Ø, Arctander P (1994) Phylogeny of the genus Pyramimonas (Prasinophyceae, Chlorophyta) inferred from the rbcL gene *J. Phycol* 30: 991-999

[17] Leliaert F, Verbruggen H, Zechman FW (2001) Into the deep: New discoveries at the base of the green plant phylogeny *Bioessays* 33: p683-692

[18] Cocquyt E (2009) Phylogeny and evolution of green algae (Fylogenie en moleculaire evolutie van groenwieren) *PhD thesis,*

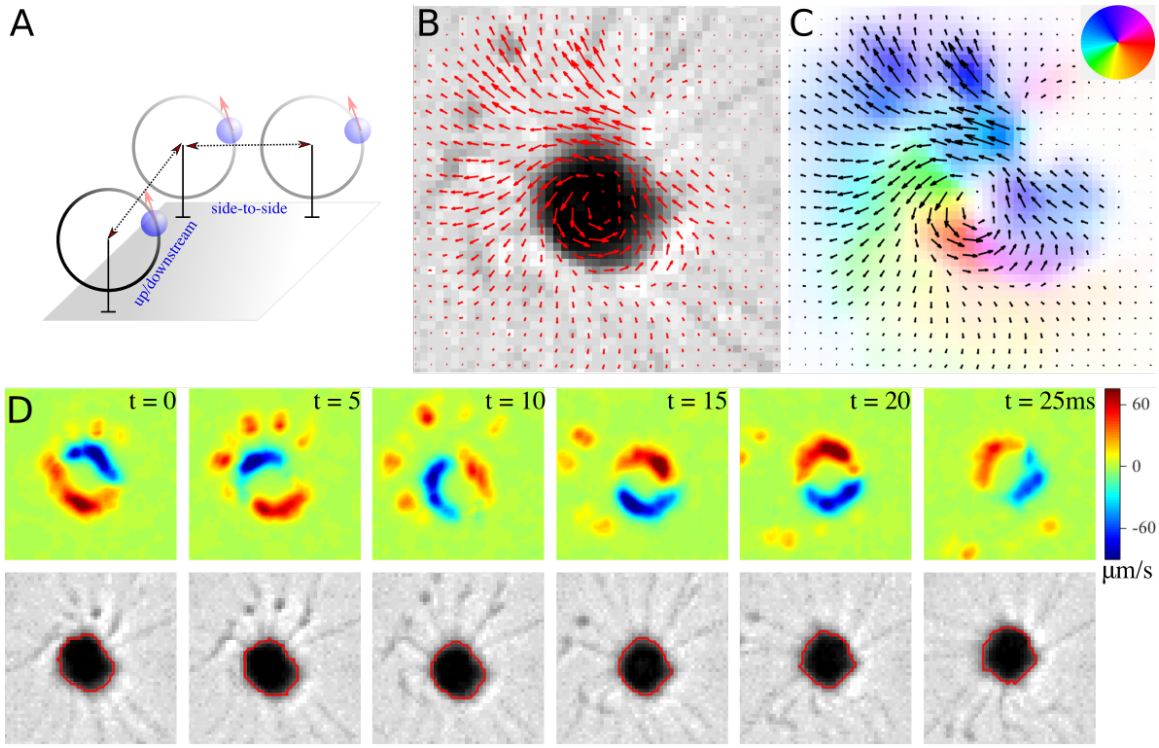

FIG. S7: Metachronism in a hexadecaflagellate. (A) The strength of hydrodynamic interactions between pairs of flagella is strongly dependent on their relative orientation. This leads to the formation of symplectic metachronal waves in a finite ring of flagellar oscillators, representing the hexadecaflagellate. (B,C) The average (optical) flow field $\langle \bar{U} \rangle$ around *P. crytoptera*. (D) Snapshots of the radial components of optical flow field.

Universiteit Ghent

[19] Demchenko E, Mikhailyuk T, Coleman AW, Proschold T (2012) Generic and species concepts in Microglena (previously the Chlamydomonas monadina group) revised using an integrative approach *Eur. J. Phycol.* 47: p264-290

[20] Buchheim M, Lemieux C, Otis C, Gutell RR, Chapman RL, Turmel M (1996) Phylogeny of the Chlamydomonadales (Chlorophyceae): A Comparison of Ribosomal RNA Gene Sequences from the Nucleus and the Chloroplast *Mol. Phylogenet. Evol* 5: p391-402

[21] Hori T, Moestrup Ø, Hoffman LR (2007) Fine structural studies on an ultraplanktonic species of Pyramimonas, P. virginica (Prasinophyceae), with a discussion of subgenera within the genus Pyramimonas *Eur. J. Phycol* 30: p219-234

[22] Harðardéttir S, Lundholm N, Moestrup Ø, Nielson TG (2014) Description of Pyramimonas diskoicola sp. nov. and the importance of the flagellate Pyramimonas (Prasinophyceae) in Greenland sea ice during the winterspring transition *Polar Biol* 37: p1479-1494

[23] Arora M, Chandrasheker A, Leliaert F, Delany J, Mesbahi E (2013) *Tetraselmis indica* (Chlorodendrophyceae, Chlorophyta), a new species isolated from salt pans in Goa, India *Eur. J. Phycol* 48: p61-78

[24] Wustman B, Melkonian M, Becker B (2004) A study of cell wall and flagella formation during cell division in the scaly green flagellate alga, Scherffelia dubia (Chlorophyta) *J. Phycol* 40: p895-910

[25] Leliaert F et al. (2012) Phylogeny and molecular evolution of the green algae. *Critical Rev. In Plant Sci.* 31: p1-46.

[26] Rumpf R, Vernon D, Schreiber D, William Birky Jr D (1996) Evolutionary consequences of the loss of photosynthesis in Chlamydomonadaceae: phylogenetic analysis of Rrn18 (18S rDNA) in 13 Polytoma strains (Chlorophyta) *J. Phycol* 32: p119-126

[27] Ueno R, Urano N, Suzuki M (2003) Phylogeny of the non-photosynthetic green micro-algal genus *Prototheca* (Trebouxiophyceae, Chlorophyta) and related taxa inferred from SSU and LSU ribosomal DNA partial sequence data *FEMS Microbio. Lett* 223: p275-280

[28] Smith DR, Hua J, Lee RW (2010) Evolution of linear mitochondrial DNA in three known lineages of Polytomella *Curr. Genet* 56: p427-438

[29] Figueroa-Martinez F, Nedelcu AM, Smith DR, Reyes-Prieto A (2015) When the lights go out: the evolutionary fate of free-living colorless green algae *New Phytologist* 206: p972-982

[30] Norris RE, Pearson BR (1975) Fine structure of Pyramimonas parkeae new species Chlorophyta Prasinophyceae. *Arch. fuer Protistenkunde* 117: p192-213.

[31] Pienaar RN, Aken ME (1985) Fine structure of Pyramimonas pseudoparkeae sp. nov. (Prasinophyte) from South Africa *J. Phycol* 21: p428-447

[32] Manton I (1968) Observations on the microanatomy of the type species of Pyramimonas (P. tetrarhynchus Schmarda). *Proc. Linn. Soc. Lond* 179: p147-152.

[33] Belcher JH (1969) Further observations on the type species of Pyramimonas (P.tetrarhynchus Schmarda) (Prasinophyceae):anexamination by light microscopy, together with notes on its taxonomy. *Bot. J. Linn. Soc.* 62: 241-253.

[34] Moestrup Ø, Hori T, Kristiansen A (1987) Fine structure of Pyramimonas octopus sp. nov., an octoflagellated benthic

species of Pyramimonas (Prasinophyceae), with some observations on its ecology *Nord. J. Bot* 7: p339-352

[35] Hori T, Moestrup Ø (1987) Ultrastructure of the flagellar apparatus in Pyramimonas octopus (Prasinophyceae).1. axoneme structure and num- bering of peripheral doublets triplets. *Protoplasma* 138: p137-148.

[36] Moestrup Ø, Hori T (1989) Ultrastructure of the flagellar apparatus in Pyramimonas octopus (Prasinophyceae) .2. flagellar roots, connecting fibers, and numbering of individual flagella in green-algae. *Protoplasma* 148: p41-56.

[37] Daugbjerg N, Moestrup Ø (1992) Ultrastructure of Pyramimonas cyr- toptera sp-nov (Prasinophyceae), a species with 16 flagella from nortrates Foxe basin, arctic Canada, including observations on growth rates. *Can. J. Bot.* 70: p1259-1273.

[38] Manton I, Parke M (1965) Observations of the fine structure of two species of Platymonas with special referennce to flagellar scales and the mode of origin of the theca *J. Mar. Biol. Ass. UK* 45: p743-754

[39] Salisbury JL, Swanson JA, Floyd GL, Hall R, Maihle NJ (1981) Ultra- structure of the flagellar apparatus of the green alga Tetraselmis subcordi- formis - with special consideration given to the function of the rhizoplast and rhizanchora. *Protoplasma* 107: p1-11.

[40] Lembi CA (1975) Fine-structure of flagellar apparatus of Carteria. *J. Phycol.* 11: p1-9.

[41] Ringo DL (1967) Flagellar motion and fine structure of flagellar apparatus in Chlamydomonas. *J. Cell Biol.* 33:p543-.

[42] Holmes JA, Dutcher SK (1989) Cellular asymmetry in *Chlamydomonas reinhardtii*, *Journal of Cell Science* 94: 273-285

[43] Kirk D (1998) *Volvox*: molecular-genetic origins of multicellularity and cellular differentiation *Developmental and Cell Biology Series, Cambridge University Press*

[44] Hoops HJ (1993) Flagellar, cellular and organismal polarity in *Volvox carteri J. Cell. Sci* 104: p105-117

[45] Lang NJ (1963) Electron-Microscopic Demonstration of Plastids in *Polytoma J. Euk. Microbiol* 10: p333-339

[46] Gaffal KP (1977) The relationship between basal bodies and the motility of *Polytoma papillatum* flagella *Experientia* 33(10): p1372-1374

[47] Brown DL, Massalski A, Paternaude R (1976) Organization of flagel- lar apparatus and associated cytoplasmic microtubules in quadriflagellate alga Polytomella agilis. *J. Cell Biol.* 69: p106-125.

[48] Harris EH (2009) The *Chlamydomonas* Sourcebook: Introduction to Chlamydomonas and its laboratory use, *Academic Press, Oxford, England*

[49] Cavalier-Smith T (1974) Basal body and flagellar development during the vegetative cell cycle and the sexual cycle of *Chlamydomonas reinhardtii J. Cell. Sci* 16: p529-556